

Broken sublattice symmetry states in Bernal stacked multilayer graphene

Chiho Yoon¹, Yunsu Jang¹, Jeil Jung^{2,*} and Hongki Min^{1†}

¹ *Department of Physics and Astronomy, Seoul National University, Seoul 08826, Korea and*

² *Department of Physics, University of Seoul, Seoul 02504, Korea*

(Dated: October 4, 2018)

We analyze the ordered phases of Bernal stacked multilayer graphene in the presence of interaction induced band gaps due to sublattice symmetry breaking potentials, whose solutions can be analyzed in terms of light-mass and heavy-mass pseudospin doublets which have the same Chern numbers but opposite charge polarization directions. The application of a perpendicular external electric field reveals an effective Hund's rule for the ordering of the sublattice pseudospin doublets in a tetralayer, while a similar but more complex phase diagram develops with increasing layer number.

1. Introduction

Ultrathin multilayer graphene has been extensively studied in the literature over the last decade as a promising platform for electronic devices [1–4] and energy storage applications [5] that take advantage of the superlattice properties of graphene. From a more fundamental physics point of view, few-layer graphenes are interesting because their band structure embodies the chiral nature of the Dirac cones near the charge neutrality point which can manifest in transport and optical experiments. Clear signatures of electron-electron interactions observed through scanning probes [6, 7] and transport experiments [8–11] have signaled interesting many-body effects. Remarkably, the predictions of interaction driven band gaps in Bernal stacked bilayer [12] and rhombohedral trilayer graphene [13] have been speculated to be accompanied by spin/valley resolved spontaneous Hall phases [14–17] for a variety of possible ground-state configurations among quasi-degenerate states. Other possible ordered phases suggested near the charge neutrality point in bilayer graphene include nematic phases with broken rotational symmetry [8, 18–23], and Fermi surface instabilities in both $\ell = 0, 1$ channels in the presence of a finite carrier doping and electric fields [24]. Recent experiments in ultraclean Bernal stacked multilayer graphenes signal the formation of electron-electron interaction driven ordered phases [25, 26].

In this paper, we analyze the nature of the electron interaction driven ordered ground-state phases in Bernal stacked tetralayer graphene subject to perpendicular external electric fields and the associated Hall conductivities that can be measured in transport experiments. We show that the electronic structure consisting of light-mass and heavy-mass band doublets follows an effective Hund's rule of the sublattice pseudospins when a perpendicular external electric field is applied, allowing to introduce qualitative changes in the associated Hall conductivities. Interestingly, in a certain range of electric fields, a ground state with a non-vanishing charge Hall con-

ductivity appears that should be measurable by conventional Hall experiments. Analysis of the ordered phases in Bernal stacked multilayer graphene beyond tetralayer acquires a more complex character due to the appearance of additional pseudospin doublets and mixing between them. Within a minimal multiband model, we show that the interaction driven band gap and broken sublattice symmetry can appear in even-layer graphenes, whereas the gaps for odd-layer graphenes are suppressed, exhibiting an even-odd effect for the energy gap size.

2. Method

We use a π -band minimal continuum model for multilayer graphene in which only nearest-neighbor intralayer hopping t_0 and interlayer hopping t_1 for the full π -bands are retained. The non-interacting Hamiltonian is

$$\hat{H}_0 = \sum_{\mathbf{k}, \sigma, \sigma'} \hat{c}_{\mathbf{k}, \sigma}^\dagger \varepsilon_{\sigma\sigma'}^{(0)}(\mathbf{k}) \hat{c}_{\mathbf{k}, \sigma'}, \quad (1)$$

where \mathbf{k} is the wavevector measured from a valley K or K' , σ is a collective index representing spin (u/d), valley, sublattice (A/B), and layer ($n = 1, 2, \dots$) degrees of freedom, $\hat{c}_{\mathbf{k}, \sigma}^\dagger$ ($\hat{c}_{\mathbf{k}, \sigma}$) is the electron creation (annihilation) operator for \mathbf{k} and σ , and $\varepsilon_{\sigma\sigma'}^{(0)}(\mathbf{k})$ is the non-interacting Hamiltonian matrix element for Bernal stacked multilayers. For the tight-binding parameters, we use the LDA parameters of graphite $t_0 = 2.598$ eV and $t_1 = 0.377$ eV [27, 28].

We include the effect of electron-electron interactions within a mean-field Hartree-Fock approximation,

$$\hat{H}_{\text{MF}} = \hat{H}_0 + \sum_{\mathbf{k}, \sigma, \sigma'} \hat{c}_{\mathbf{k}, \sigma}^\dagger \varepsilon_{\sigma\sigma'}^{(\text{HF})}(\mathbf{k}) \hat{c}_{\mathbf{k}, \sigma'}. \quad (2)$$

The matrix element of the Hartree-Fock term is given by

$$\begin{aligned} \varepsilon_{\sigma\sigma'}^{(\text{HF})}(\mathbf{k}) &= \delta_{\sigma\sigma'} \sum_{\mathbf{k}', \sigma'} V_{nn'}(0) \langle \hat{c}_{\mathbf{k}', \sigma'}^\dagger \hat{c}_{\mathbf{k}', \sigma'} \rangle \\ &\quad - \delta_{\sigma\sigma'} \sum_{\mathbf{k}'} V_{nn'}(|\mathbf{k} - \mathbf{k}'|) \langle \hat{c}_{\mathbf{k}', \sigma'}^\dagger \hat{c}_{\mathbf{k}', \sigma} \rangle, \end{aligned} \quad (3)$$

*Electronic address: jeil.jung@gmail.com

†Electronic address: hmin@snu.ac.kr

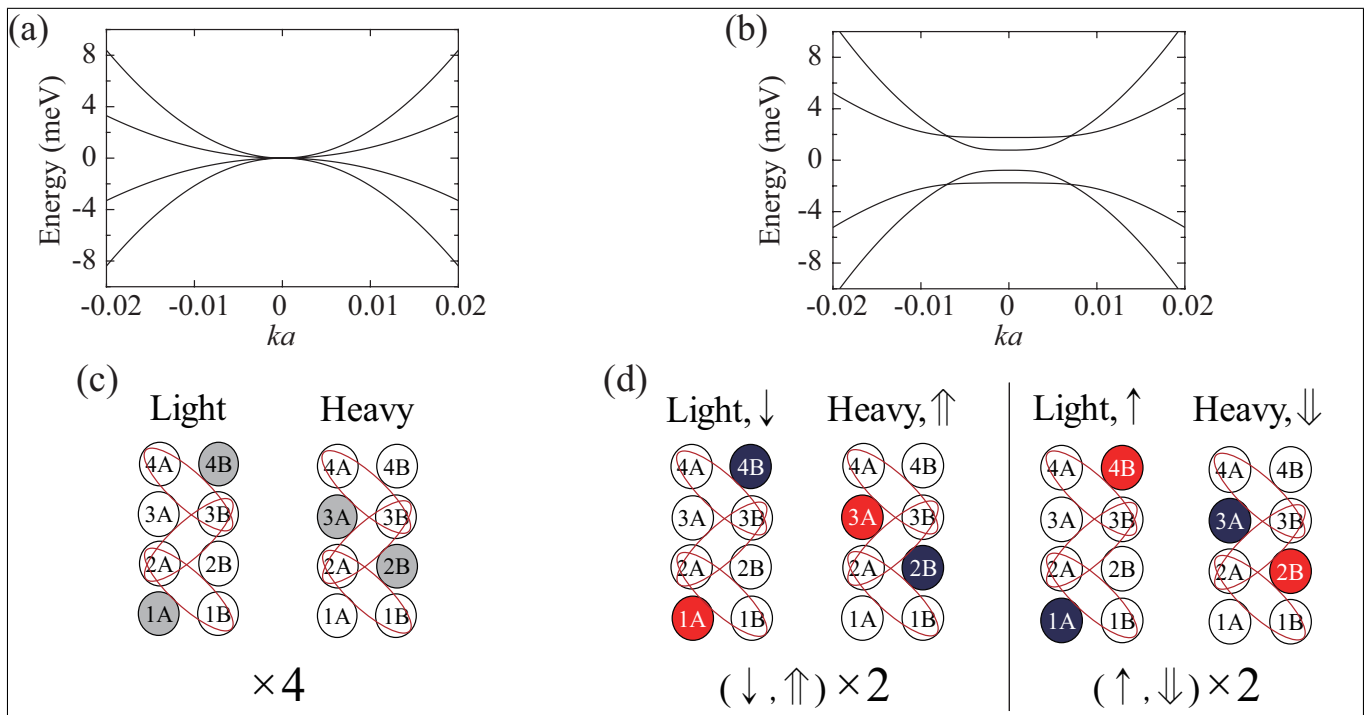


FIG. 1: Electronic structure and zero-energy wavefunction configurations near the K or K' valley for ABAB tetralayer graphene obtained respectively from (a), (c) the non-interacting continuum model and (b), (d) a self-consistent Hartree-Fock calculation. Two pseudospin doublets are labeled by “Light” or “Heavy” depending on their effective mass of the energy band. In the case of non-interacting model, all four spin/valley flavors have the same wavefunction configuration with localized wavefunctions on the gray sublattices, as shown in (c). When electron-electron interactions are turned on, the sublattice symmetry is broken for both doublets transferring charges either from A to B sublattices or vice versa, as indicated in red (positive charge) and blue (negative charge) color in (d). The (\downarrow, \uparrow) and (\uparrow, \downarrow) labels represent two possible configurations of opposite charge polarization towards the top and bottom layers corresponding to the light and heavy mass bands.

where n and s denote the layer and spin, respectively. $V_{nn'}(q) = \frac{2\pi e^2}{\epsilon_r q} e^{-|n-n'|qd}$ is the Coulomb interaction matrix where $d = 3.35 \text{ \AA}$ is the interlayer separation and ϵ_r is the background dielectric constant. The first and second terms in the right-hand side of Eq. (3) represent the classical Hartree and exchange Fock contributions, respectively. Note that the Hartree terms reduce to potential differences between the layers when we take the proper limit at $q = 0$. Here we take a rather small value of the interaction strength $\alpha \equiv \frac{e^2}{\epsilon_r \hbar v}$, where $v = \frac{\sqrt{3}}{2} \frac{t_0 a}{\hbar}$ is the Fermi velocity of monolayer graphene and $a = 2.46 \text{ \AA}$ is the lattice constant, to effectively account for the overestimation of the exchange by long-ranged Coulomb repulsion in a Hartree-Fock theory that misses out the screening effects of π and σ orbitals in graphene. (Simple screening models such as the static Thomas-Fermi approximation for the exchange interaction do not change the qualitative picture on the sublattice symmetry breaking presented in this paper.) The specific value $\alpha = 0.1$ is adopted to match the experimentally observed gap size in bilayer graphene [7, 10, 11].

To overcome computational challenges posed by the absence of analytic form of wavefunctions in multilayer graphene, we use the rotational transformation method

[29] in which the wavefunction at an arbitrary angle is obtained by a stacking dependent unitary transformation of the wavefunction at a specific angle. Moreover, we omit the inter-valley interaction which is negligibly small, and each one of the four spin/valley flavors are treated independently.

3. Results

3.1. Interaction-driven gapped phases in Bernal stacked tetralayer graphene

The experimentally observed band gap in Bernal stacked tetralayer graphene suggests the presence of electron-electron interaction driven symmetry breaking [25, 26]. Here, we show that the band gap opens due to interaction driven sublattice symmetry breaking and its internal structure consists of light-mass and heavy-mass band doublets whose charge densities polarize towards opposite out-of-plane directions. A sufficiently strong perpendicular external electric field can flip their polarization directions in the order of increasing effective mass values.

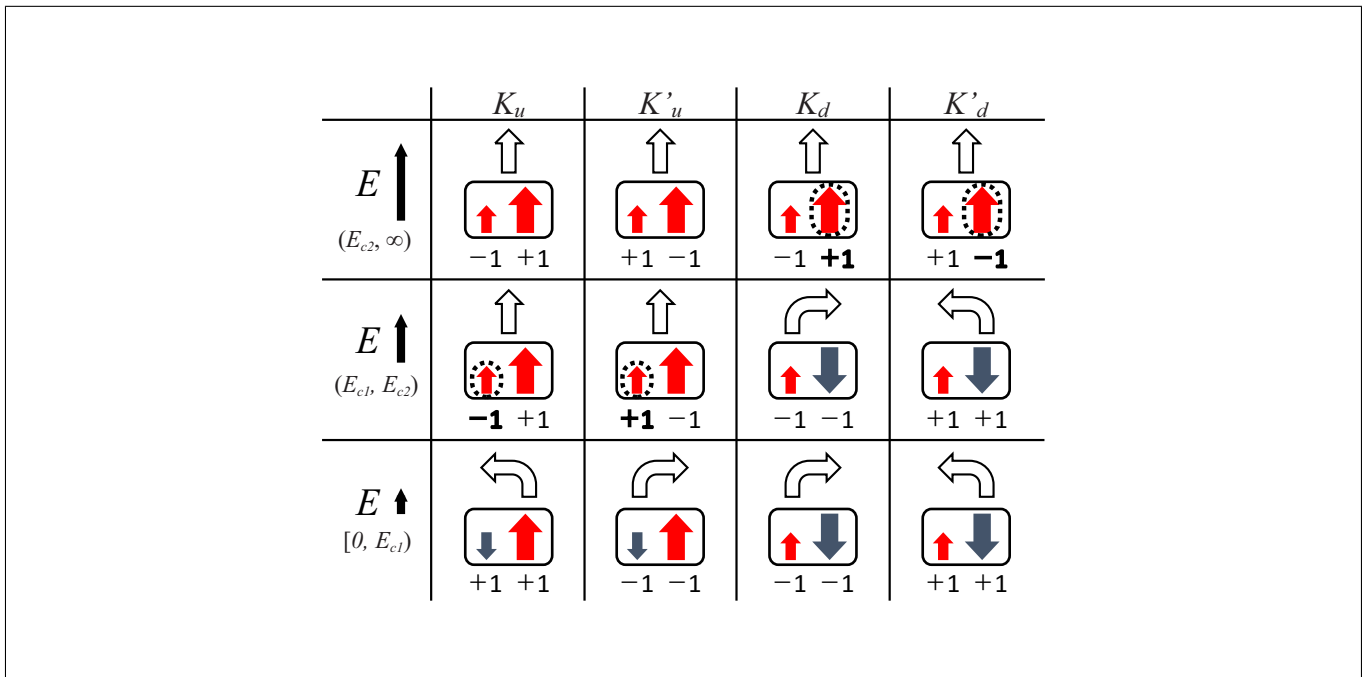


FIG. 2: The evolution of the layer antiferromagnetic state under a perpendicular external electric field, keeping the flavor degeneracy of the system. Arrows in the square box and numbers below the box at each spin/valley flavor represent pseudospin polarizations and corresponding Chern numbers, respectively, whereas the arrows above the box indicate the corresponding net current directions expected in the Hall measurement. The change in the charge polarization by applying a perpendicular electric field is denoted by the dashed circle.

In Fig. 1, we show a comparison of the non-interacting and Hartree-Fock energy band structures, and corresponding ground-state wavefunction amplitudes and charge polarizations near the Fermi energy. The electronic structure of Bernal stacked multilayer graphene can be understood from the chiral decomposition rules of arbitrarily stacked multilayers [33, 34] where the ABAB tetralayer is the simplest example involving more than one massive band. In the absence of electron-electron interactions, the low-energy band structure of ABAB stacking is described by two bilayer-like pseudospin doublets with different effective masses, whose wavefunctions near the Fermi energy are mainly localized at outer layer (1A, 4B) and inner layer (2B, 3A) sublattice sites that define the pseudospin basis for the light and heavy mass bands, respectively, as shown in Fig. 1(c). In the presence of electron-electron interactions, the sublattice symmetry of the two-fold degenerate pseudospin doublets in the occupied bands is broken by transferring charge either from A to B sublattices or vice versa for both doublets (but not from A to B for one doublet and from B to A for other doublet), resulting in the gapped band structure with the same *sublattice* polarization direction.

Sublattice symmetry breaking in tetralayer graphene can be considered as the generalization of the case of bilayer graphene system, which has one pseudospin (per spin and valley) whose direction is out-of-plane as a result of the electron-electron interactions [12]. For each spin/valley flavor, the charge polarizations of the light-

mass and heavy-mass band doublets can be represented as (\downarrow, \uparrow) or (\uparrow, \downarrow) , where the first (second) arrow in the parenthesis denotes the charge polarization for the light (heavy) mass band. The charge polarizations for light and heavy bands point in opposite directions but towards the same sublattices, leading to same sign Chern numbers $(+1, +1)$ or $(-1, -1)$, as shown in the Fig. 1(d). Note that the Chern number changes its sign at the opposite valley. We will discuss later on the states with the same polarization directions such as (\downarrow, \downarrow) or (\uparrow, \uparrow) with a vanishing net Chern number for a single spin/valley flavor, which are possible in the presence of an external electric field. Thus, we can expect a variety of ground states as a function of an external electric field, where different types of Hall conductivities can result depending on the polarization of light-mass and heavy-mass band doublets for each flavor.

Similar to the discussions for pseudospin magnetism in bilayer graphene [12] we can classify the different states into flavor antiferro, ferri, and ferro states. Flavor antiferro states have two flavors in (\downarrow, \uparrow) configuration and the other two in (\uparrow, \downarrow) configuration at zero field, so that no net charge polarization exists. Flavor antiferro states can be further classified depending on their Hall conductivities [35]. Flavor ferro states have all four flavors in the same pseudospin configuration. The flavor ferri states have one distinct flavor with respect to other three. Since the number of (\downarrow, \uparrow) and (\uparrow, \downarrow) configurations are different in flavor ferro and ferri states at zero field, non-zero

net charge polarization exists for these states. From the Hartree energy cost considerations, the metastable states with the lowest total energy are expected to be flavor antiferro when there is no external electric field perpendicular to the graphene layers.

3.2. Electric field induced “Hund’s rule” and Hall effects

Now let us consider the effect of a perpendicular external electric field that can introduce a richer phase diagram. The presence of an electric field is able to reorganize the charge polarization of the sublattice pseudospins in each spin/valley flavor. (Here we evolve a pseudospin configuration under an electric field without changing its antiferro, ferri or ferro character keeping the same flavor degeneracy. The lowest total energy state among them is discussed in the following section.) We begin by considering the flavor antiferro state consisting of $(\downarrow, \uparrow) \times 2$ and $(\uparrow, \downarrow) \times 2$ at zero field. When an external electric field is increased beyond the first critical field of $E_{c1} = 0.025$ mV/Å, the polarization of the light-mass band changes its sign first due to smaller interaction-induced sublattice potential compared with that for the heavy-mass band, resulting in the $(\uparrow, \uparrow) \times 2$ and $(\uparrow, \downarrow) \times 2$ configuration. A second critical electric field of $E_{c2} = 0.879$ mV/Å is able to flip all pseudospins leading to a ground state with four identical copies of the band doublets $(\uparrow, \uparrow) \times 4$, and thus resulting in flavor ferro state. Figure 2 schematically illustrates this process and resulting transport properties in one of the flavor antiferro states, the layer antiferromagnetic phase, assuming a spin dependent but valley independent sublattice potential [35]. Thus, polarizations of the pseudospin doublets arising from the interaction induced sublattice symmetry breaking are aligned by the external electric field in the order of increasing effective mass. It can be shown that this simple “Hund’s rule” type pseudospin ordering applies also to flavor ferri and ferro states, whose detailed discussion can be found in the Supplemental Material [35].

3.3. Generalization to thicker multilayer stacks

In Bernal stacked multilayer graphene beyond tetralayer, there are several additional factors that influence electronic structure near the Fermi level due to the increased number of pseudospin doublets and their interactions. Here, we intend to provide a qualitative picture of the electronic structure expected in Bernal stacked multilayer graphene in the presence of electron-electron interactions and perpendicular external electric fields using a minimal continuum model for the band Hamiltonian.

In Bernal stacked multilayer graphene, the low-energy effective theory is described by a set of bilayer-like doublets for even-number of layers, while an additional

monolayer-like doublet is found for odd-number of layers. The major difference in the energy gap between even- and odd-layer graphenes originates from the existence of the monolayer-like doublet in odd layered multilayers [30–33]. Unlike bilayer-like doublets, monolayer-like doublets are much more robust to the interaction-induced sublattice symmetry breaking and tend to remain gapless [12], thus the gaps of odd-layer graphenes are much smaller than those of even-layer graphenes.

In Fig. 3 (a), we show the energy band gap as a function of the number of layers in the absence of electric field. For even number of layers the energy gap opens due to interactions and decreases as the number of layers increases, whereas for odd number of layers the energy gap almost remains closed. Note that the energy gap for odd number of layers is not exactly zero (except for a single layer) and the energy gap for both odd and even layers saturate as the number of layers increases. It is important to note that these remnant gaps are due to simplification in the minimal model and expected to be closed when remote hopping terms and screening are considered.

Restricting our attention to even-layer graphene, we summarize in Fig. 3 (b) the effect of a perpendicular electric field in the ground-state configurations. In general, the lowest total energy state varies from a flavor antiferro state with zero net charge polarization via a partially polarized state, and eventually to fully polarized flavor ferro state. Interestingly, for an appropriate external electric field range, the flavor ferri state (or “All” state [15–17]), which exhibits non-zero Hall conductivities of all flavors can be achieved not only in rhombohedral but also in Bernal stacked multilayer graphene. Since the total energies are almost degenerate, we expect that domains of different pseudospin configurations will form in a disordered sample [36]. Considering the large number of pseudospin flavors in tetralayers and beyond, it is also expected that a large variety of topological domain walls will arise at the interface between the ordered pseudospin domains.

4. Discussion

We identified the structure of the electron-electron interaction driven ordered phases in Bernal stacked multilayer graphene based on the polarization of the pseudospin doublets belonging to electronic bands with distinct effective masses. Our analysis rests on a number of simplifying assumptions such as: neglect of remote hopping terms and the energy difference between the dimer and non-dimer sites Δ , and the absence of screening and correlations in our interaction model. In our minimal model for the band Hamiltonian, only the nearest intralayer and interlayer hopping is considered for simplicity in order to conserve the rotational symmetry of the Hamiltonian. As the number of layers becomes larger, however, the remote hopping terms cannot be omitted

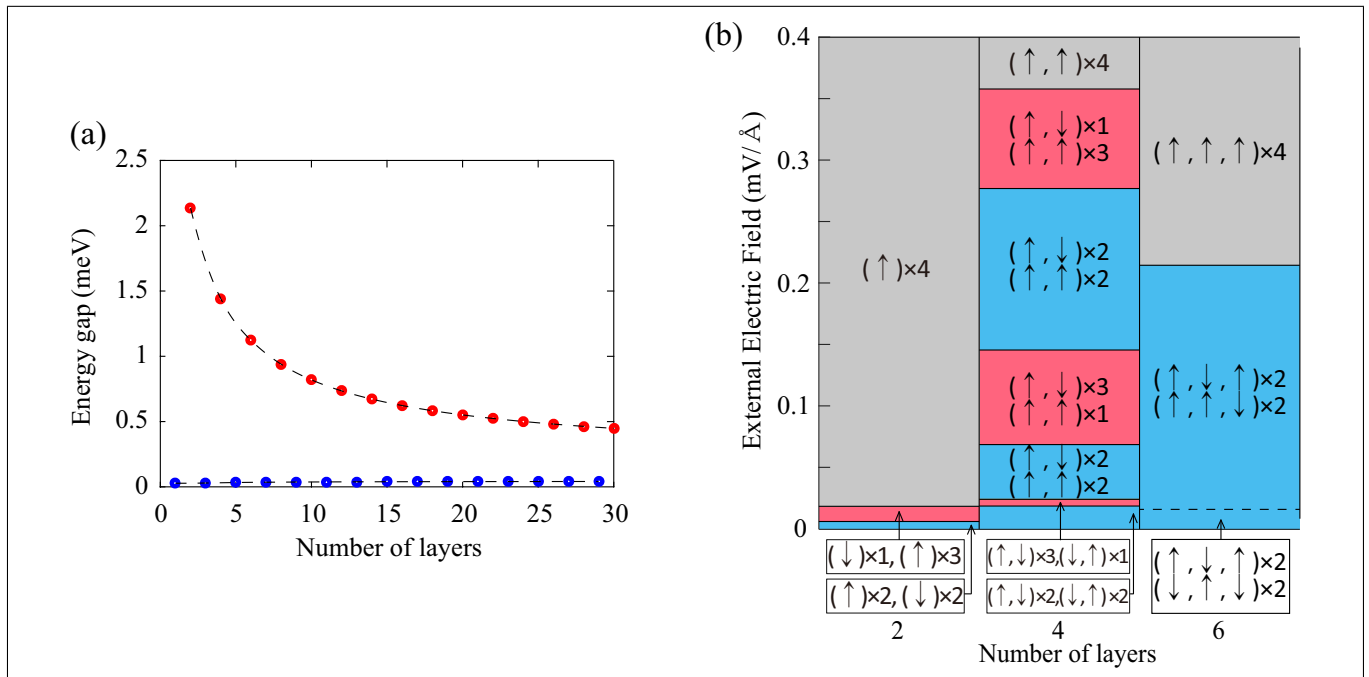


FIG. 3: (a) Energy band gap as a function of the number of layers in the absence of a perpendicular electric field. The energy gaps of even (odd) number of layers are denoted by red (blue) circles. (b) The lowest total energy states in the presence of electric field. Flavor antiferro, ferri, and ferro states are colored in blue, red, and gray, respectively. The pseudospin polarization directions are written in increasing effective mass order.

for an accurate description of the band structure. Each remote hopping term plays a different role in multilayer graphene, but in general, it distorts the chiral character of the low energy band near the K or K' point reducing the density of states near the Fermi energy. Since the energy gap originates from the interplay of chirality and electron-electron interaction, the energy gap is expected to become smaller when the remote hopping terms are considered. Once the energy gap is closed or becomes narrower, the screening effect due to the Coulomb interaction begins to play a significant role, in a particularly notable manner for odd-layer graphenes. For even-layer graphenes, larger interaction induced gaps open. When the gap size sets the dominant energy scale relative to the remote hopping energies, the basic picture presented in this paper should be valid at least qualitatively. It has been proposed that the electron-electron interactions will induce strains that suppress the remote interlayer coupling terms such as the γ_2 hopping [26]. The assumption of weakened remote hopping terms in few layer systems would make the minimal model an adequate ground for the analysis of interaction effects. As the number of layers increases towards the graphite limit, however, it is expected that the energy gap should show a progressive

decrease until it eventually closes.

In summary, we provide a simple and comprehensive picture for the interaction induced ordered states in Bernal stacked multilayer graphene. We analyze the ground-state configurations and associated Hall conductivities that can result from the combined presence of electron-electron interactions and perpendicular external fields that could serve as guidance to future experiments.

5. Acknowledgments

Authors thank A. H. MacDonald, F. Zhang and J.-J. Su for helpful discussions. This research was supported by Basic Science Research Program through the National Research Foundation of Korea (NRF) funded by the Ministry of Education under Grant No. 2015R1D1A1A01058071. J.J. acknowledges financial support from the Korean NRF through the grant NRF-2016R1A2B4010105. C.Y. acknowledges the financial support of the NRF grant funded by the Korean Government (NRF-2016H1A2A1907780).

[1] A. H. Castro Neto, F. Guinea, N. M. R. Peres, K. S. Novoselov, and A. K. Geim, Rev. Mod. Phys. **81**, 109

(2009).

[2] S. Das Sarma, S. Adam, E. H. Hwang, and E. Rossi, Rev.

- Mod. Phys. **83**, 407 (2011).
- [3] D.N. Basov, M.M. Fogler, A. Lanzara, F. Wang, and Y. Zhang, Rev. Mod. Phys. **86**, 959 (2014).
- [4] H. Raza (Ed.), *Graphene Nanoelectronics*, Springer (2012).
- [5] H. Ji, X. Zhao, Z. Qiao, J. Jung, Y. Zhu, Y. Lu, L. L. Zhang, A. H. MacDonald, and R. S. Ruoff, Nat. Commun. **5**, 3317 (2014).
- [6] R. T. Weitz, M. T. Allen, B. E. Feldman, J. Martin, and A. Yacoby, Science **330**, 812 (2010).
- [7] B. E. Feldman, J. Martin, and A. Yacoby, Nat. Phys. **5**, 889 (2009).
- [8] A. S. Mayorov, D. C. Elias, M. Mucha-Kruczynski, R. V. Gorbachev, T. Tudorovskiy, A. Zhukov, S. V. Morozov, M. I. Katsnelson, V. I. Fal'ko, A. K. Geim, and K. S. Novoselov, Science **333**, 860 (2011).
- [9] J. Velasco Jr., L. Jing, W. Bao, Y. Lee, P. Kratz, V. Aji, M. Bockrath, C. N. Lau, C. Varma, R. Stillwell, D. Smirnov, F. Zhang, J. Jung, and A. H. MacDonald, Nat. Nanotech. **7**, 156 (2012).
- [10] F. Freitag, J. Trbovic, M. Weiss, and C. Schonenberger, Phys. Rev. Lett. **108**, 076602 (2012).
- [11] A. Veligura, H. J. van Elferen, N. Tombros, J. C. Maan, U. Zeitler, and B. J. van Wees, Phys. Rev. B **85**, 155412 (2012).
- [12] H. Min, G. Borghi, M. Polini, and A. H. MacDonald, Phys. Rev. B **77**, 041407(R) (2008).
- [13] J. Jung and A. H. MacDonald, Phys. Rev. B **88**, 075408 (2013).
- [14] R. Nandkishore and L. Levitov, Phys. Rev. Lett. **104**, 156803 (2010).
- [15] F. Zhang, J. Jung, G. A. Fiete, Q. Niu, and A. H. MacDonald, Phys. Rev. Lett. **106**, 156801 (2011).
- [16] J. Jung, F. Zhang, and A. H. MacDonald, Phys. Rev. B **83**, 115408 (2011).
- [17] F. Zhang, Synth. Met. **210**, 9 (2015).
- [18] K. Sun, H. Yao, E. Fradkin, and S. A. Kivelson, Phys. Rev. Lett. **103**, 046811 (2009).
- [19] F. Zhang, H. Min, M. Polini, and A. H. MacDonald, Phys. Rev. B **81**, 041402(R) (2010).
- [20] O. Vafek and K. Yang, Phys. Rev. B **81**, 041401(R) (2010).
- [21] O. Vafek, Phys. Rev. B **82**, 205106 (2010).
- [22] R. Nandkishore and L. Levitov, Phys. Rev. B **82**, 115124 (2010).
- [23] Y. Lemonik, I. L. Aleiner, C. Toke, and V. I. Falko, Phys. Rev. B **82**, 201408(R) (2010).
- [24] J. Jung, M. Polini and A. H. MacDonald, Phys. Rev. B **91**, 155423 (2015).
- [25] A. L. Grushina, D.-K. Ki, M. Koshino, A. A.L. Nicolet, C. Faugeras, E. McCann, M. Potemski, and A. F. Morpurgo, Nat. Commun. **6**, 6419 (2015).
- [26] Y. Nam, D.-K. Ki, M. Koshino, E. McCann, and A. F. Morpurgo, 2D Mater. **3**, 045014 (2016).
- [27] J.-C. Charlier, X. Gonze, and J.-P. Michenaud, Phys. Rev. B **43**, 4579 (1991).
- [28] J. Jung and Allan H. MacDonald, Phys. Rev. B **89**, 035405 (2014).
- [29] Y. Jang, E. H. Hwang, A. H. MacDonald, and H. Min, Phys. Rev. B **92**, 041411(R) (2015).
- [30] F. Guinea, A. H. Castro Neto, and N. M. R. Peres, Phys. Rev. B **73**, 245426 (2006).
- [31] S. Latil and L. Henrard, Phys. Rev. Lett. **97**, 036803 (2006).
- [32] B. Partoens and F. M. Peeters, Phys. Rev. B **75**, 193402 (2007).
- [33] H. Min and A. H. MacDonald, Phys. Rev. B **77**, 155416 (2008).
- [34] H. Min and A. H. MacDonald, Prog. Theor. Phys. Suppl. **176**, 227 (2008).
- [35] See Supplemental Material for details of the flavor antiferro, ferri and ferro states in tetralayer graphene, the ground-state configurations for 6-layer graphene, and the effect of remote hopping terms.
- [36] X. Li, F. Zhang, Q. Niu, and A. H. MacDonald, Phys. Rev. Lett. **113**, 116803 (2014).

Supplemental Material: Broken sublattice symmetry states in Bernal stacked multilayer graphene

Chiho Yoon¹, Yunsu Jang¹, Jeil Jung², and Hongki Min¹

¹ *Department of Physics and Astronomy, Seoul National University, Seoul 08826, Korea and*

² *Department of Physics, University of Seoul, Seoul 02504, Korea*

I. FLAVOR ANTIFERRO STATES IN TETRALAYER GRAPHENE

From the Hartree energy cost considerations, the metastable states with the lowest total energy are expected to be flavor antiferro when there is no external electric field perpendicular to the graphene layers. Within the energetically more favorable flavor antiferro states, we classify different Hall phases [1, 2]: layer antiferromagnetic (LAF) phase with the spin dependent but valley independent sublattice potential, quantum spin Hall (QSH) phase with both the spin and valley dependent sublattice potential, and quantum anomalous Hall (QAH) phase with the valley dependent but spin independent sublattice potential, as schematically shown in Fig. 1.

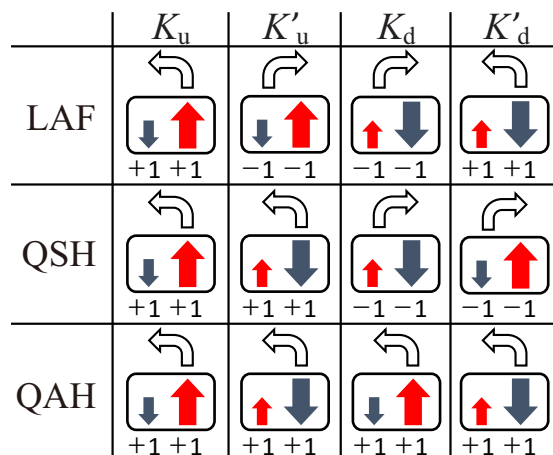


FIG. 1: Schematic picture of the ground-state configuration and corresponding spontaneous Hall effect at zero external electric field for three possible flavor antiferro states: LAF, QSH and QAH. Arrows in the square box and numbers below the box at each spin/valley flavor represent pseudospin polarizations and corresponding Chern numbers, respectively, whereas the arrows above the box indicate the corresponding net current directions expected in the Hall measurement.

The internal arrangement of the sublattice pseudospins has a direct impact on the Hall transport properties of the system. Whenever the charge polarization direction flips, the associated Chern number changes its sign due to the change in the sublattice potential in the doublet. We distinguish the spin Hall (SH), valley Hall (VH), charge Hall (CH), and spin resolved valley Hall (SV) contributions of the conductivities. From the Chern numbers $C_{v,s}$ ($v = K, K'$ and $s = u, d$) of the pseudospin doublets at each valley/spin flavor, the various quantum Hall conductivities can be evaluated as

$$\sigma_{\text{SH}} = \frac{e^2}{h} (C_{K,u} - C_{K,d} + C_{K',u} - C_{K',d}), \quad (1a)$$

$$\sigma_{\text{VH}} = \frac{e^2}{h} (C_{K,u} + C_{K,d} - C_{K',u} - C_{K',d}), \quad (1b)$$

$$\sigma_{\text{CH}} = \frac{e^2}{h} (C_{K,u} + C_{K,d} + C_{K',u} + C_{K',d}), \quad (1c)$$

$$\sigma_{\text{SV}} = \frac{e^2}{h} (C_{K,u} - C_{K,d} - C_{K',u} + C_{K',d}). \quad (1d)$$

Table I shows the resulting Hall conductivities for three distinct energy degenerate configurations (LAF, QSH, QAH) of the flavor antiferro phase.

TABLE I: Spontaneous quantum Hall conductivities in units of e^2/h for the antiferro states in Bernal stacked tetralayer graphene under a perpendicular external electric field. Here, $E_{c1} = 0.025$ mV/Å and $E_{c2} = 0.879$ mV/Å.

E_{ext}	LAF				QSH				QAH			
	SH	VH	CH	SV	SH	VH	CH	SV	SH	VH	CH	SV
E_{c2}	0	0	0	0	0	0	0	0	0	0	0	0
E_{c1}	0	-4	0	4	4	-4	0	0	0	-4	4	0
0	0	0	0	8	8	0	0	0	0	0	8	0
$-E_{c1}$	0	4	0	4	4	4	0	0	0	4	4	0
$-E_{c2}$	0	0	0	0	0	0	0	0	0	0	0	0

II. FLAVOR FERRI AND FERRO STATES IN TETRALAYER GRAPHENE

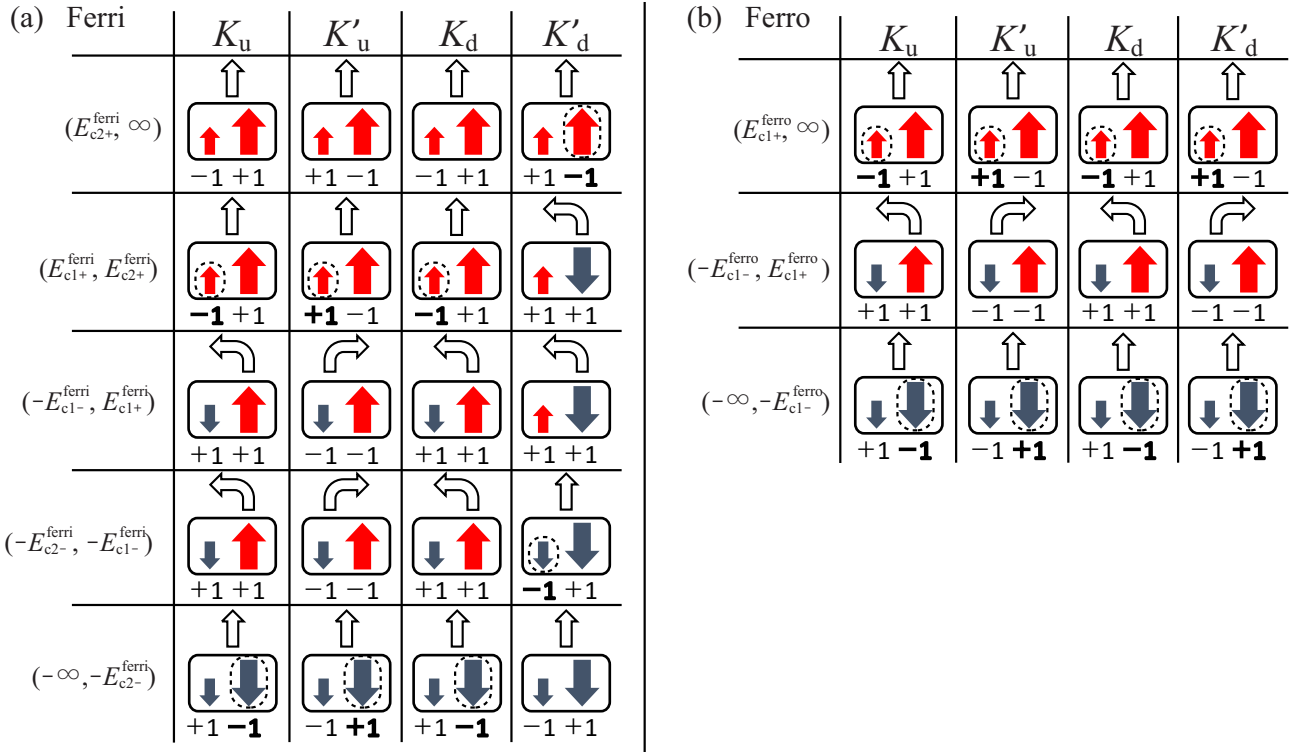


FIG. 2: The evolution of ABAB tetralayer graphene under a perpendicular external electric field for (a) a flavor ferri state with the minority pseudospin configuration (\uparrow, \downarrow) on K'_d and (b) a flavor ferro state with (\downarrow, \uparrow) for all four flavors. Arrows in the square box and numbers below the box at each spin/valley flavor represent pseudospin polarizations and corresponding Chern numbers, respectively, whereas the arrows above the box indicate the corresponding net current directions expected in the Hall measurement. The change in the charge polarization by applying a perpendicular electric field is denoted by the dashed circle.

As demonstrated in the main text, the ground-state configurations of tetralayer graphene and their field dependence can be clearly explained by the effective “Hund’s rule”. The evolution of a flavor ferri state with the minority pseudospin configuration on K'_d and that of a flavor ferro state under a perpendicular external electric field are depicted in Fig. 2. The corresponding Chern numbers for each state are represented in Tab. II. Note that in zero external electric field, there are eight ferri states (from the two possible choice of minority configuration between (\uparrow, \downarrow) and (\downarrow, \uparrow) on four possible spin/valley flavors) and two ferro states (from the two possible choice of majority configuration).

As shown in Table II, in the case of ferri states, all the types of Hall coefficients are non-zero for $-E_{c2-}^{\text{ferri}} < E < E_{c2+}^{\text{ferri}}$. This is the reason why the ferri state is also called “All” state [1–3]. Also note that only the valley Hall coefficients

TABLE II: Spontaneous quantum Hall conductivities in units of e^2/h under a perpendicular external electric field in ABAB tetralayer for the ferri and ferro states in Fig. 2. Here, $E_{c1+}^{\text{ferri}} = 0.019$, $E_{c2+}^{\text{ferri}} = 0.943$, $E_{c1-}^{\text{ferri}} = 0.031$, and $E_{c2-}^{\text{ferri}} = 0.815$ meV/Å for the ferri state, whereas $E_{c1+}^{\text{ferro}} = 0.013$ and $E_{c1-}^{\text{ferro}} = 0.753$ meV/Å for the ferro state.

E	Ferri				E	Ferro			
	SH	VH	CH	SV		SH	VH	CH	SV
E_{c2+}^{ferri}	0	0	0	0	E_{c1+}^{ferro}	0	0	0	0
E_{c1+}^{ferri}	-2	-2	2	2	0	0	8	0	0
0	-4	4	4	4	$-E_{c1-}^{\text{ferro}}$	0	0	0	0
$-E_{c1-}^{\text{ferri}}$	-2	6	2	2					
$-E_{c2-}^{\text{ferri}}$	0	0	0	0					

change their signs in the opposite field direction. In the case of ferro states, only the valley Hall coefficients are non-zero for $-E_{c1-}^{\text{ferro}} < E < E_{c1+}^{\text{ferro}}$.

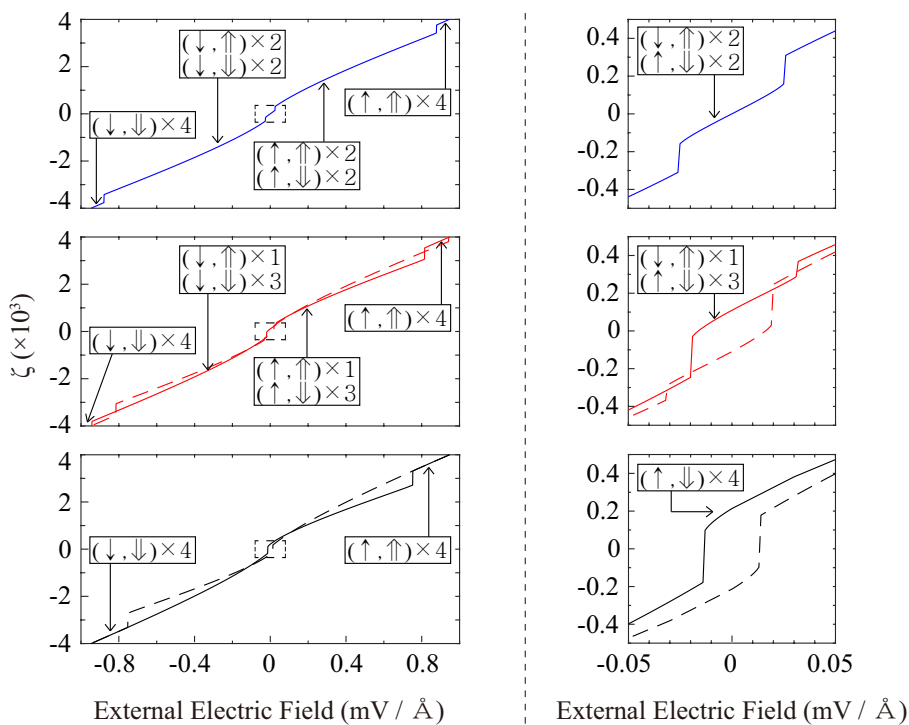


FIG. 3: (Left) External field dependence of the total charge polarization ζ defined in Eq. (2) for flavor antiferro (top), ferri (middle) and ferro (bottom) states. The solid and dashed lines indicate evolutions of states from two different initial states with reversed polarization direction for each pseudospin. For each solid line, the pseudospin configurations are depicted. (Right) Zoomed view of the dashed rectangular area in the left panel.

Figure 3 shows the external field dependence of the total charge polarization for flavor antiferro, ferri and ferro states tracing a single metastable configuration. Here, we define the total charge polarization ζ in tetralayers taking into account the layer separations as

$$\zeta = \frac{\frac{3}{2}n_4 + \frac{1}{2}n_3 - \frac{1}{2}n_2 - \frac{3}{2}n_1}{n_4 + n_3 + n_2 + n_1}, \quad (2)$$

where n_i is the electron density at i -th layer. Note that in the case of ferri and ferro states, the evolution of states depends on the initial condition and the sweep direction of the field, exhibiting hysteretic behavior associated with the broken sublattice symmetry at zero field, which is analogous to the bilayer graphene system [4].

TABLE III: Charge polarizations and corresponding Chern numbers in the presence of a perpendicular electric field in Bernal stacked 6-layer graphene for the LAF state. The pseudospins are written in increasing effective mass order from the left to the right. Here, $E_{c1}^{(6)} = 0.017$, $E_{c2}^{(6)} = 0.251$, and $E_{c3}^{(6)} = 0.281$ meV/Å. Red arrows indicate flipped pseudospin polarizations with field.

E	Flavor I (K_u, K'_u)			Flavor II (K_d, K'_d)			Chern Number					
	K_u	K'_u	K_d	K'_d	K_u	K'_u	K_d	K'_d	K_u	K_d	K'_u	K'_d
$E_{c3}^{(6)}$	↑	↑	↑	↑	↑	↑	1	1	-1	-1		
$E_{c2}^{(6)}$	↑	↑	↑	↑	↑	↓	1	-1	-1	1		
$E_{c1}^{(6)}$	↑	↓	↑	↑	↑	↓	3	-1	-3	1		
0	↑	↓	↑	↓	↑	↓	3	-3	-3	3		
$-E_{c1}^{(6)}$	↓	↓	↑	↓	↑	↓	1	-3	-1	3		
$-E_{c2}^{(6)}$	↓	↓	↑	↓	↓	↓	1	-1	-1	1		
$-E_{c3}^{(6)}$	↓	↓	↓	↓	↓	↓	-1	-1	1	1		

TABLE IV: Spontaneous quantum Hall conductivities in units of e^2/h for the antiferro states in Bernal stacked 6-layer graphene under a perpendicular external electric field.

E_{ext}	LAF				QSH				QAH			
	SH	VH	CH	SV	SH	VH	CH	SV	SH	VH	CH	SV
$E_{c3}^{(6)}$	0	4	0	0	0	4	0	0	0	4	0	0
$E_{c2}^{(6)}$	0	0	0	4	4	0	0	0	0	0	4	0
$E_{c1}^{(6)}$	0	4	0	8	8	4	0	0	0	4	8	0
0	0	0	0	12	12	0	0	0	0	0	12	0
$-E_{c1}^{(6)}$	0	-4	0	8	8	-4	0	0	0	-4	8	0
$-E_{c2}^{(6)}$	0	0	0	4	4	0	0	0	0	0	4	0
$-E_{c3}^{(6)}$	0	-4	0	0	0	-4	0	0	0	-4	0	0

III. GROUND-STATE CONFIGURATIONS FOR 6-LAYER GRAPHENE

Similarly as tetralayer graphene, the low-energy band structure of Bernal stacked 6-layer graphene (ABABAB) at low energies is described by three bilayer-like pseudospin doublets with different masses. Because of the sublattice symmetry breaking, charge polarizations of the three pseudospins have alternating directions, $(\downarrow, \uparrow, \downarrow)$ or $(\uparrow, \downarrow, \uparrow)$ where arrows in the parenthesis represent the charge polarization of pseudospins with increasing effective mass order. The corresponding Chern numbers are $(+1, +1, +1)$ or $(-1, -1, -1)$ because of the same sign of sublattice potential generated by the sublattice symmetry breaking. Similarly, we can understand the ground-state configurations of 8-layer graphene (ABABABAB) as $(\downarrow, \uparrow, \downarrow, \uparrow)$ or $(\uparrow, \downarrow, \uparrow, \downarrow)$ with the Chern numbers $(+1, +1, +1, +1)$ or $(-1, -1, -1, -1)$ at zero field.

Table III shows the external field dependence of the ground-state configurations in the LAF state for 6-layer graphene. In Tab. IV, the corresponding Hall conductivities are calculated for the three possible antiferro states, respectively. When the external electric field E_{ext} is zero, pseudospins with increasing effective mass have alternating charge polarization directions for 6-layer graphene, which is consistent with the tetralayer case. As E_{ext} increases, each pseudospin flips from the one with lighter effective mass following the Hund's rule. As the number of layers increases, however, there are deviations from this rule in the intermediate field region resulting from the greater complexity of the intermediate states and the interaction between the bands near the Fermi energy.

IV. EFFECT OF THE REMOTE HOPPING TERMS

In even-layer graphenes, the energy gap is the dominant energy scale, thus when the gap is large enough, the effect of other energy scales associated with remote hopping terms could be negligible and the basic picture presented in this paper remains valid at least qualitatively. However, when the remote hopping terms are not negligible compared to the energy gap, the ground state is no longer described by the sublattice symmetry breaking and the effective Hund's rule, and the detailed ground state configurations will be determined by combined effects of the remote hopping terms and screening. Figure 4 shows the phase diagram between the gap dominant and remote-hopping dominant regions as a function of the interaction strength α and the next-nearest interlayer coupling between non-dimer sites γ_2 in

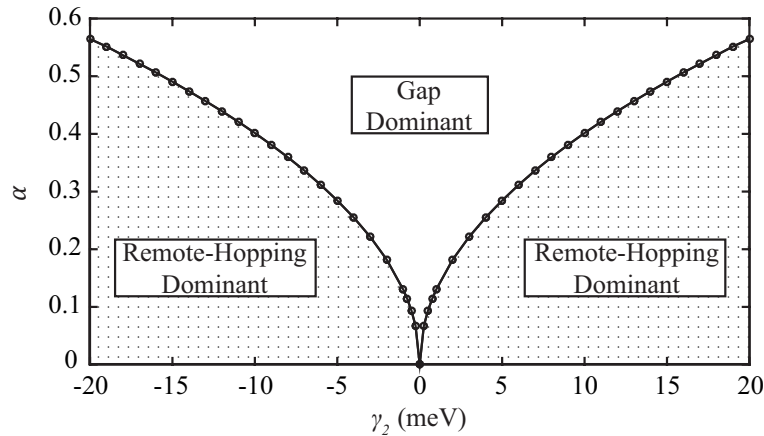


FIG. 4: The phase diagram for the ground state configuration of tetralayer graphene on α and γ_2 plane. Here, the gap (remote-hopping) dominant region denotes a region where the ground state is (not) described by the sublattice symmetry breaking and the effective Hund's rule.

tetralayer graphene, ignoring the other remote hopping terms for simplicity. In the gap (remote-hopping) dominant region, the ground state is (not) described by the sublattice symmetry breaking and the effective Hund's rule. As expected, broken sublattice symmetry occurs at large α and small size of γ_2 . If we adopt the proposal that the remote hopping terms in multilayer graphene are different from those in graphite and are suppressed by interaction induced strains [5], the use of the minimal model for the band Hamiltonian would be justified. Considering that $\alpha \sim 1$ for conventional SiO_2 substrates and $\alpha \sim 2.6$ for suspended samples for the dielectric environment, we expect a fair chance that the gap dominant region prevails over the remote hopping dominant region. The fact that a rather weaker $\alpha \sim 0.1$ in our modeling gives a reasonable description of the experiments indicates that the quantitative value of the band gap contains a combined effect of interaction screening and band Hamiltonian effects that should be accounted for in a more complete theory.

-
- [1] F. Zhang, J. Jung, G. A. Fiete, Q. Niu, and A. H. MacDonald, Phys. Rev. Lett. **106**, 156801 (2011).
 - [2] J. Jung, F. Zhang, and A. H. MacDonald, Phys. Rev. B **83**, 115408 (2011).
 - [3] F. Zhang, Synth. Met. **210**, 9 (2015).
 - [4] H. Min, G. Borghi, M. Polini, and A. H. MacDonald, Phys. Rev. B **77**, 041407(R) (2008).
 - [5] Y. Nam, D.-K. Ki, M. Koshino, E. McCann, and A. F. Morpurgo, 2D Mater. **3**, 045014 (2016).